Role of a Glutamate Bridge Spanning the Dimeric Interface of Human Manganese Superoxide Dismutase[†,‡]

Patrick S. Quint,[§] John F. Domsic,[||] Diane E. Cabelli,[⊥] Robert McKenna,*[,||] and David N. Silverman*[,§,||]

Department of Pharmacology and Therapeutics and Department of Biochemistry and Molecular Biology, University of Florida, Gainesville, Florida 32610, and Department of Chemistry, Brookhaven National Laboratory, Upton, New York 11973

Received December 16, 2007; Revised Manuscript Received February 15, 2008

ABSTRACT: The function in the structure, stability, and catalysis of the interfaces between subunits in manganese superoxide dismutase (MnSOD) is currently under scrutiny. Glu162 in homotetrameric human MnSOD spans a dimeric interface and forms a hydrogen bond with His163 of an adjacent subunit which is a direct ligand of the manganese. We have examined the properties of two site-specific mutants of human MnSOD in which Glu162 is replaced with Asp (E162D) and Ala (E162A). The X-ray crystal structures of E162D and E162A MnSOD reveal no significant structural changes compared with the wild type other than the removal of the hydrogen bond interaction with His163 in E162A MnSOD. In the case of E162D MnSOD, an intervening solvent molecule fills the void created by the mutation to conserve the hydrogen bond interaction between His163 and residue 162. These mutants retain their tetrameric structure and their specificity for manganese over iron. Each has catalytic activity in the disproportionation of superoxide that is typically 5–25% of that of the wild-type enzyme and a level of product inhibition greater by approximately 2-fold. Differential scanning calorimetry indicates that the hydrogen bond between Glu162 and His163 contributes to the stability of MnSOD, with the major unfolding transition occurring at 81 °C for E162A compared to 90 °C for wild-type MnSOD. These results suggest that Glu162 at the tetrameric interface in human MnSOD supports stability and efficient catalysis and has a significant role in regulating product inhibition.

Manganese superoxide dismutase (MnSOD)[1] catalyzes the disproportionation of superoxide to produce O_2 and H_2O_2 (*1, 2*). Human MnSOD is a homotetramer of 22 kDa subunits, a dimer of dimers, with two structurally unique interfaces, one dimeric and one tetrameric (Figure 1). The function in the catalysis, stability, and structure of these interfaces is uncertain. Many residues at the dimeric interface are conserved between prokaryotes and eukaryotes (*3, 4*). The tetrameric interface, generally associated with eukaryotic MnSOD, may play a role in stability; for example, tetrameric human MnSOD has a major thermal unfolding transition at 90 °C, while that measured for the dimeric *Escherichia coli* enzyme is 76 °C (*5, 6*). This role is further supported by the presence of a tetrameric interface in MnSOD of the thermophilic prokaryotes *Thermus thermophilus* and *Pyrobaculum aerophilum* (*7, 8*).

Several studies have investigated the roles of the dimeric and tetrameric interfaces in terms of stability and catalysis. Human MnSOD containing the I58T mutation at the tetrameric interface is predominantly dimeric in solution with its major unfolding temperature decreased to 76 °C with loss of activity (*9*). The Y166F mutation at the dimeric interface of human MnSOD results in an up to 40-fold loss of activity and a major unfolding temperature of 74 °C, indicating a significant role for the dimeric interface in both catalysis and stability (*10*). ^{19}F NMR and deuterium−hydrogen exchange studies showed that certain residues at the dimeric interface of human MnSOD have less conformational mobility than residues at the tetrameric interface (*11*).

In this work, we examine the role of a glutamate residue that spans the dimeric interface and forms a hydrogen bond with a histidine that is a ligand of the metal in an adjacent residue. In MnSOD from *E. coli*, this is Glu170. Its replacement in E170A results in enhanced dissociation of the dimer and a very interesting change in metal specificity since this mutant binds iron exclusively and no longer has catalytic activity (*12*). The active site regions of MnSOD from humans and *E. coli* are very closely superimposable (*3, 13*). The equivalent mutation in human MnSOD, E162A, is a

[†] This work was supported by NIH Grant GM 54903. Pulse radiolysis studies were carried out at the Center for Radiation Chemical Research at Brookhaven National Lab which is supported by the US Department of Energy (DE-AC02-98CH10886).

[‡] Coordinates and structure factors have been deposited in the Protein Data Bank as entries 3C3T and 3C3S.

* To whom correspondence should be addressed. D.N.S.: Department of Pharmacology, College of Medicine, University of Florida, Box 100267, Gainesville, FL 32610; phone, (352) 392-3556; fax, (352) 392-9696; e-mail, silvrmn@ufl.edu. R.M.: Department of Biochemistry and Molecular Biology, College of Medicine, University of Florida, Box 100245, Gainesville, FL 32610; phone, (352) 392-5696; fax, (352) 392-3422; e-mail, rmckenna@ufl.edu.

[§] Department of Pharmacology and Therapeutics, University of Florida.

[||] Department of Biochemistry and Molecular Biology, University of Florida.

[⊥] Brookhaven National Laboratory.

[1] Abbreviations: MnSOD, manganese superoxide dismutase; E162A MnSOD, site-specific mutant of MnSOD with Glu162 replaced with Ala; rmsd, root-mean-square deviation.

10.1021/bi7024518 CCC: $40.75
Published on Web 03/29/2008

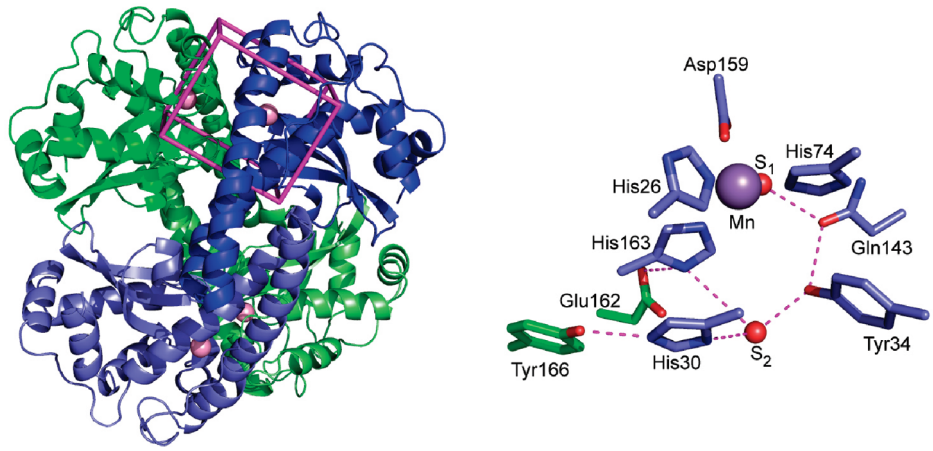

FIGURE 1: Structure of human wild-type MnSOD [produced using coordinates from Protein Data Bank (PDB) entry 1LUV (*37*)]. The left panel shows the homotetrameric organization with blue and green used for the quaternary structure of the subunits and (as indicated by the magenta box) the dimeric interface (between blue and green monomers), including the region of an active site. The right panel is a close-up of the active site structure. The amino acids of adjacent subunits are colored blue and green, and the manganese and solvent molecules are depicted as purple and red spheres, respectively. The dashed lines represent a hydrogen bonded network emanating from the manganese-bound solvent molecule of one monomer (blue) to Tyr166 of an adjacent subunit (green). This figure was created using PyMol (www.pymol.org).

topic of this investigation. In contrast to the results with the corresponding mutant of *E. coli* MnSOD, the human E162A MnSOD is found in this work to retain its specificity for manganese, to have appreciable catalytic activity, and to retain its tetrameric structure. This is part of a growing body of evidence that emphasizes that although the human and bacterial MnSODs have similar active site structures, other properties can be quite different. This includes the extent of product inhibition, which dominates catalysis by human MnSOD at high superoxide concentrations but is slight in *E. coli* MnSOD (*14*).

MATERIALS AND METHODS

Site-Directed Mutagenesis. Mutants were generated with the Stratagene (La Jolla, CA) QuikChange Site-Directed Mutagenesis Kit in a Perkin-Elmer (Foster City, CA) GeneAmp PCR System 2400. The plasmid of wild-type MnSOD contained in the pTrc99A vector was used as the template. PCR was performed using as primers specific oligonucleotides (Sigma-Genosys, The Woodlands, TX) containing the desired mutations. The PCR products were digested with the restriction enzyme *Dpn*I and transformed into supercompetent XL-1 cells for selection. The plasmid containing the mutation of interest was isolated using the plasmid mini prep kit from Qiagen, and the mutation was corroborated by DNA sequencing of the entire coding region (ICBR, University of Florida). The plasmid containing the desired mutation was then transformed into QC774 cells from *E. coli*. This particular strain lacks the genes that encode endogenous FeSOD (*SodB*$^-$) and MnSOD (*SodA*$^-$) (*15*).

Expression and Purification of Human MnSOD. Cells were grown in Luria-Bertani broth supplemented with 6 mM $MnCl_2$ and ampicillin for selection. Cultures were grown to an OD_{580} of 0.8 absorbance unit and then induced with IPTG. Cells were centrifuged and then lysed. The lysate was heat treated at 60 °C for 15 min to select for MnSOD. Following heat treatment, the lysate was spun and the supernatant was dialyzed against three exchanges of 20 mM Tris (pH 8.2) and 50 μM EDTA. The dialysate was purified using a Q-Sepharose anion exchange column (Pharmacia). Protein concentrations were determined by UV spectrometry at 280 nm using a Beckman Coulter DU 800 spectrometer at 25 °C and pH 7.8 ($\epsilon_{280} = 40500\ M^{-1}\ cm^{-1}$) (*6*).

Visible Absorption. The visible spectrum for human MnSOD exhibited a broad absorption with a maximum at 480 nm ($\epsilon_{480} = 610\ M^{-1}\ cm^{-1}$) (*16*). Profiles for pH dependence were determined by measuring the absorption at 480 nm at values of pH varying from 6.5 to 11.5. Enzyme samples were diluted 1:1 (~500 μM enzyme) in a buffer containing 200 mM MES and 200 mM TAPS, and the pH was adjusted using KOH.

Pulse Radiolysis. Pulse radiolysis experiments were performed at Brookhaven National Laboratory using a 2 MeV van de Graaff accelerator to produce superoxide directly in solution. Superoxide radicals were formed by exposing aqueous, air-saturated solutions to a high-dose electron pulse according to methods described by Schwarz (*17*). Up to 45 μM superoxide was produced in solution. Enzyme solutions contained 2 mM buffer (MOPS at pH 6.5–8.0, TAPS at pH 8.0–9.0, or CAPS at pH 9.0–10.0), 50 μM EDTA, and 30 mM formate to scavenge hydroxyl radicals. The reactions were monitored spectrophotometrically using a Cary 210 spectrophotometer at 25 °C by following changes in the absorbance of superoxide ($\epsilon_{260} = 2000\ M^{-1}\ cm^{-1}$) (*18*) or by following enzyme absorbance (*19*).

Determination of Manganese and Iron Content. A Perkin-Elmer 308 flame atomic absorption spectrometer was utilized to determine the manganese concentration. A multi-ion lamp with a three-slit burner was used, and absorption was measured at 279 nm. Typical occupancies for manganese in the active sites of E162D and E162A MnSOD ranged from 54 to 90%. Iron content was measured by ABC Research Corp. (Gainesville, FL) and was determined to account for roughly 2% of the total metal in E162D and E162A MnSOD. The manganese concentration was used as the active enzyme concentration for measurements of catalysis.

Table 1: Rate Constants k_1–k_4 (eqs 1−4) for the Catalysis and Inhibition of Human Wild-Type MnSOD and Its Mutants

	k_1 (μM^{-1} s^{-1})	k_2 (μM^{-1} s^{-1})	k_3 (μM^{-1} s^{-1})	k_4 (s^{-1})
wild type[a]	1500	1100	1100	120
E162D[b]	355 ± 33	133 ± 16	215 ± 20	40 ± 4
E162A[b]	63 ± 4	50 ± 4	87 ± 8	30 ± 3
Y166F[c]	200	200	200	270

[a] From ref (*37*). [b] In 2 mM TAPS (pH 7.7), 50 mM EDTA, and 30 mM formate at 25 °C. [c] From ref (*10*).

Crystallography. Crystals of E162D and E162A MnSOD were grown using a precipitant solution of 3 M ammonium sulfate containing 100 mM imidazole and 100 mM malate at pH 7.8–8.2 using the vapor diffusion hanging drop method. Hexagonal crystals with dimensions of approximately 0.2 mm × 0.2 mm × 0.3 mm grew at room temperature (RT) within 1 week and were magenta in color. Diffraction data were collected from visually selected single crystals wet mounted in quartz capillaries (Hampton Research) on an R-AXIS IV^{++} image plate (IP) system with Osmic mirrors and a Rigaku HU-H3R CU rotating anode operating at 50 kV and 100 mA. A 0.3 mm collimator was used with a crystal to IP distance of 220 mm and a 2θ angle of 0°. The frames were collected using a 0.3° oscillation angle with an exposure time of 5 min/frame at RT. Both data sets were indexed using DENZO and scaled and reduced with SCALEPACK (*20*). Useful Bragg diffraction data were collected to 2.3 and 2.5 Å resolution for the E162D and E162A MnSOD crystals, respectively.

To prevent model bias, the E162D and E162A MnSOD crystal data sets were phased using the human wild-type MnSOD structure (*21*) (PDB entry 2ADQ) from which the residue at position 162 was replaced with an alanine and the active site manganese had been removed. The structures were phased and refined using CNS (*22*). Refinement cycling (using rigid body, simulated annealing for the first cycle, minimization, and individual *B*-factor refinement) was done in conjunction with rounds of manual model building using COOT for molecular modeling (*23*). The refined model statistics are given in Table 2. The refined models and structure factor files have been deposited with the Protein Data Bank as entries 3C3T and 3C3S for E162D and E162A MnSOD, respectively.

Differential Scanning Calorimetry. E162D and E162A MnSOD samples were buffered in 20 mM potassium phosphate (pH 7.8) at a concentration of 1 mg/mL. The protein concentration for acquisition of wild-type MnSOD data was 0.5 mg/mL. Both the sample and reference solutions were degassed for 10 min before being scanned from 25 to 110 °C at a rate of 1 °C/min (Microcal VP-DSC). A buffer blank was subtracted from the final protein scan, and a cubic baseline was fit to the profile. Changes in heat capacity (ΔC_p) for the unfolding peaks were corrected by fitting a reversible, non-two-state model with two components. Baseline correction and peak fitting were performed using Origin (Microcal Software, Northampton, MA).

RESULTS

Amino acid Glu162 at the dimeric interface of human MnSOD was replaced with Asp and Ala. Atomic absorption spectroscopy of extensively dialyzed samples of the E162D mutant [20 mM phosphate (pH 7.8)] showed Mn occupancy at the active site was 88% and Fe occupancy was 2%. For the E162A mutant, the occupancy was 54% for Mn and 2% for Fe. Both mutants were tetramers under experimental conditions as determined by nondenaturing PAGE. Human wild-type Mn^{3+}SOD as well as E162D and E162A Mn^{3+}SOD exhibit a characteristic visible absorbance with a maximum at 480 nM (ϵ_{480} = 610 M^{-1} cm^{-1} for the wild type) (*16*). The reduced form Mn^{2+}SOD has no appreciable absorbance in the visible region (ϵ_{480} < 30 M^{-1} cm^{-1}). The pH profile for molar absorptivity (480 nm) for wild-type human Mn^{3+}SOD was fit by a single ionization with a pK_a of 9.2 ± 0.1 (Figure 2). Replacement of Glu162 with Asp resulted in a pK_a of 8.7 ± 0.2, whereas replacement with Ala increased the value to 10.1 ± 0.1 (Figure 2).

Table 2: Diffraction Data and Refinement Statistics for Human E162D and E162A MnSOD

	E162D	E162A
space group	$P6_122$	$P6_122$
unit cell parameters (Å)	a = 81.3, c = 241.7	a = 81.3, c = 242.5
resolution (Å)	20–2.2 (2.28–2.20)[a]	20–2.5 (2.59–2.50)[a]
no. of unique reflections	23358	15609
completeness (%)	93.5 (90.7)[a]	90.1 (92.7)[a]
R_{sym}[b] (%)	11.2 (19.6)[a]	11.4 (21.0)[a]
$I/\sigma(I)$	28.2	22.2
R_{cryst}[c] (%)	17.58	17.7
R_{free}[d] (%)	20.09	22.2
no. of protein atoms	3106	3100
no. of water molecules	175	103
rmsd for bond lengths (Å)	0.006	0.006
rmsd for bond angles (deg)	1.248	1.325
average *B* (main/side/solvent)	21.7/24.4/35.3	26.8/28.2/33.4
Ramachandran plot (%)		
most favored regions	91.2	91.8
additional allowed regions	7.6	7.0
generously allowed regions	1.2	1.2

[a] Data in parentheses are for the highest-resolution shell. [b] $R_{sym} = (\sum|I - \langle I\rangle|/\sum\langle I\rangle) \times 100$. [c] $R_{cryst} = (\sum||F_o| - |F_c||/\sum|F_o|) \times 100$. [d] R_{free} is calculated the same as R_{cryst}, except with the 5% of the reflection data omitted from refinement.

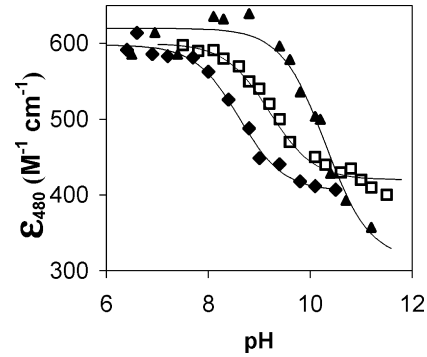

FIGURE 2: pH profile for molar absorptivity at 480 nm for (□) human wild-type Mn^{3+}SOD, (◆) E162D Mn^{3+}SOD, and (▲) E162A Mn^{3+}SOD. Data were fit to a single ionization with pK_a values of 8.7 ± 0.2, 9.2 ± 0.1, and 10.1 ± 0.1 for E162D, wild-type, and E162A Mn^{3+}SOD, respectively. Solutions contained 200 mM MES and TAPS at 25 °C.

Catalysis. MnSOD catalyzes the disproportionation of superoxide through a two-step process in which the active site metal cycles between the Mn^{3+} and Mn^{2+} states concomitant with oxidation and reduction of superoxide, as shown in the mechanism of eqs 1 and 2 (*2, 24, 25*). This representation reflects the suggestion that the solvent ligand of the metal in Mn^{3+}(OH)SOD takes up a proton upon

reduction of the metal (eq 1) (*26*). Equations 3 and 4 represent the formation and dissociation, respectively, of a product-inhibited complex which has been characterized by a zero-order phase in catalysis (*25, 27, 28*).

$$Mn^{3+}(OH)SOD + O_2^{\bullet -} + H^+ \xrightarrow{k_1} Mn^{2+}(H_2O)SOD + O_2 \quad (1)$$

$$Mn^{2+}(H_2O)SOD + O_2^{\bullet -} + H^+ \xrightarrow{k_2} Mn^{3+}(OH)SOD + H_2O_2 \quad (2)$$

$$Mn^{2+}(H_2O)SOD + O_2^{\bullet -} \xrightarrow{k_3} Mn^{3+}(O_2^{2-})SOD \quad (3)$$

$$Mn^{3+}(O_2^{2-})SOD + H^+ + H_2O \xrightarrow{k_4} Mn^{3+}(OH)SOD + H_2O_2 \quad (4)$$

Estimation of the rate constants of eqs 1−4 was carried out by measuring the rate of change of absorbance of $O_2^{\bullet -}$ and of enzyme species after the generation of $O_2^{\bullet -}$ by pulse radiolysis, as described in previous reports (*19, 28*). The resulting values of k_1-k_4 for catalysis by E162A and E162D MnSOD measured at pH 7.7 are given in Table 1, where they are compared with the values of other variants of human MnSOD. The rate constant k_1 was determined by the decrease in absorption of superoxide at 260 nm which is characterized by a first-order phase of catalysis that is relatively uninhibited followed by a zero-order, product-inhibited phase (*25, 27, 29*). A second method for determining k_1 was to measure changes in absorption at 480 nm under single-turnover conditions when there is a molar excess of enzyme (*19*). Values of k_1 for the two methods were in agreement. After addition of 1 molar equiv of H_2O_2 to reduce the active site manganese to Mn^{2+}, pulse radiolysis to generate superoxide caused an increase in absorption at 480 nm which gave an estimate for k_2 at earlier time points and k_4 for the later part of the curve. The product-inhibited complex has a characteristic absorption at 420 nm (*27, 28*); k_3 was measured from the increase in absorption at 420 nm and corresponding decrease at 480 nm (*19*). Figure 3 shows typical data generated for the measurement of k_3.

The values of k_1-k_4 describing catalysis by human wild-type MnSOD were independent of pH in the range of 7−9.5 with a slight decrease above pH 9.5 (*6, 28*). However, for E162D MnSOD, the rate constant k_1 for catalysis was pH-dependent (Figure 4) and could be fit to a single ionization with maxima of 355 ± 33 μM^{-1} s^{-1} and a pK_a of 8.7 ± 0.2. The values of k_2 and k_3 for E162D exhibited some decrease from the values at pH 7.7 given in Table 1 to values near 50 μM^{-1} s^{-1} at pH 9.9 but were not adequately described by a single ionization, and the rate constant k_4 describing the dissociation of the product-inhibited complex exhibited no pH dependence. The rate constants k_1-k_3 for catalysis by E162A MnSOD exhibited no pH dependence, but k_4 was decreased 10-fold as the pH decreased from 8 to 10, from 30 ± 3 to 3 ± 1 s^{-1}, but could not be fit to a single ionization (data not shown).

The rate constant k_0/[E] describing the product-inhibited, zero-order region of catalysis at steady state for E162D MnSOD was 270 s^{-1} and was mostly pH independent, though there was a decrease at higher pH (to 190 s^{-1} at pH 8.3). The E162A mutant exhibited a more extensive decrease

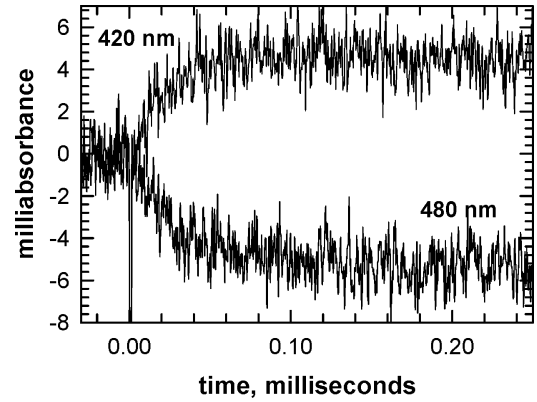

FIGURE 3: Change in absorbance at 420 and 480 nm over a millisecond time scale after generation of 5.6 μM superoxide by pulse radiolysis in a solution containing 120 μM E162D MnSOD buffered by 2 mM TAPS (pH 8.35) with 50 μM EDTA and 30 mM sodium formate at 25 °C. The disappearance at 480 nm was observed when the oxidized sample was pulsed in the absence of peroxide. The growth at 420 was observed when, prior to pulsing, the sample was reduced with H_2O_2. Both the decrease and increase in absorbance at 480 and 420 nm were fit to first-order processes. The increase at 420 gave a rate of 14 ms^{-1}, from which a value of k_3 (eq 3) was determined.

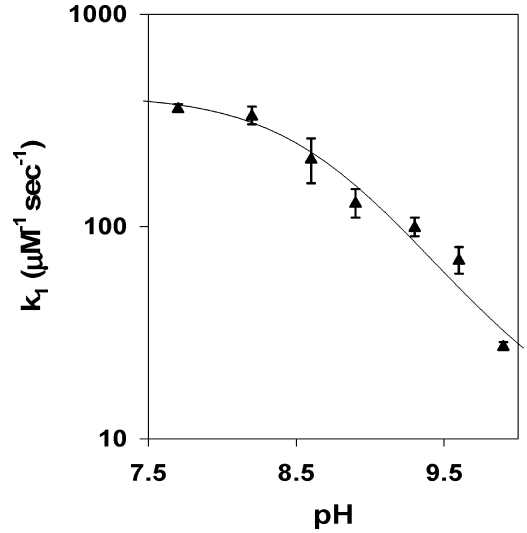

FIGURE 4: pH profile for k_1 in catalysis of the disproportionation of superoxide by E162D MnSOD. Solutions contained 2 μM enzyme, 2 mM buffer (see Materials and Methods), 50 μM EDTA, and 30 mM sodium formate at 25 °C. A single ionization was fit to the data with a value for pK_a of 8.7 ± 0.2. Each data point is the mean and standard deviation of three or four points.

with pH. The value for k_0/[E] at pH 7.7 was 190 s^{-1}, while at pH 8.4, it decreased to 18 s^{-1}; however, here again the decrease was not adequately fit to a single ionization. For comparison, the value of k_0/[E] is near 500 s^{-1} for wild-type MnSOD and is pH-independent (*28, 29*).

Structure of MnSOD Mutants. The human MnSOD mutants E162D and E162A crystallized in hexagonal space group $P6_122$ under similar crystallization conditions (see Materials and Methods) (diffraction data statistics are given in Table 2). Both mutants were homodimers in the crystallographic asymmetric unit with the eukaryotic tetramer formed from a crystal 2-fold symmetry operator. The structures of the two mutants superimposed well on human

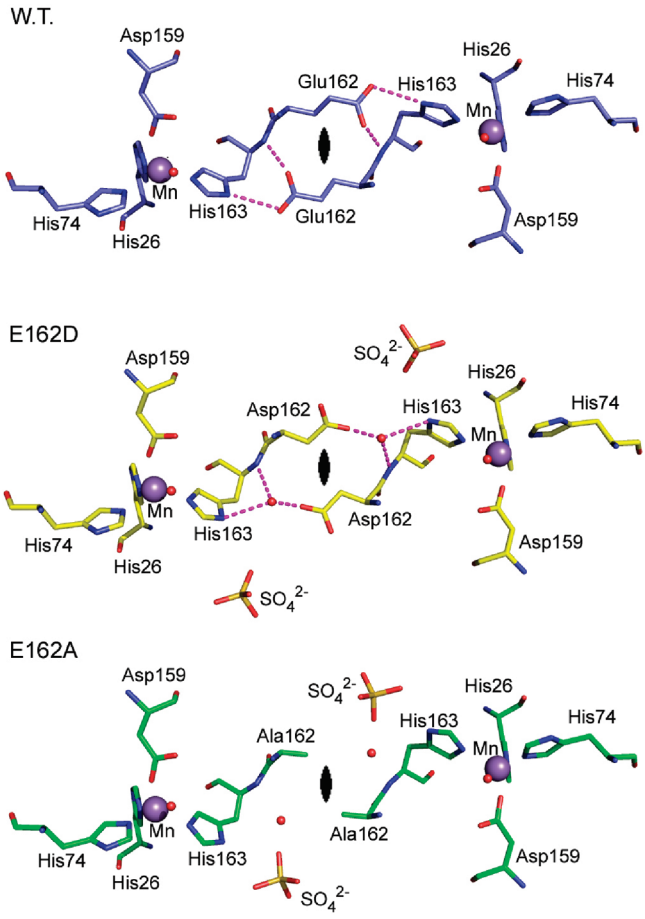

FIGURE 5: Structures of (top) human wild-type MnSOD, (middle) E162D MnSOD, and (bottom) E162A MnSOD viewed down the dimeric interface. The large purple and small red spheres depict the manganese and solvent oxygen atoms, respectively. In E162D MnSOD, a solvent molecule was observed bridging the hydrogen bond interaction between Asp162 and His163, and in E162D and E162A MnSOD, sulfate molecules were found in the proximity of Asp162. The dashed lines represent hydrogen bonds. This figure was created using PyMol (www.pymol.org).

wild-type MnSOD with a rmsd of 0.2 Å for both E162D and E162A MnSOD.

A major difference that appears in the mutated MnSOD structures is an alteration of the hydrogen bond interaction between Glu162 and His163 found in wild-type MnSOD (Figure 5). The active site structure of E162D MnSOD retains an interaction between the carboxylate of Asp162 and His163 through an intervening water molecule (Figure 5). This interaction is absent in the structure of E162A (Figure 5). It may be interesting that in both structures of the mutant there is a putative ordered sulfate molecule near the void made by the replacement of Glu162 which has apparently opened up a solvent channel in the tetramer structure of both mutants.

Thermal Stability. Differential scanning calorimetry was used to determine major thermal transition temperatures for the unfolding of E162D and E162A MnSOD in 20 mM phosphate buffer (pH 7.8). The calorimetric data for both mutants were the composite of three experiments averaged and normalized to a non-two-state model with two components. E162D MnSOD exhibited two peaks, and these melting temperatures were quite similar to those observed for the wild type. The average thermal inactivation temperature for E162D MnSOD was 72 °C, and the unfolding temperature was 88 °C (Figure S1 of the Supporting Information). These values for wild-type human MnSOD are reported to be 68 and 90 °C, respectively (*9*). Our own determination of the wild-type MnSOD inactivation and unfolding transitions yielded values of 72 and 94 °C, respectively (Figure S2 of the Supporting Information). Calorimetry of E162A MnSOD exhibited a split peak with values for the transition temperatures at 77 and 81 °C (Figure S3 of the Supporting Information).

DISCUSSION

The focus of this study is the role of Glu162 in human MnSOD, a prominent residue that spans the dimeric interface and is a second-shell ligand of the manganese. Using two site-specific mutants, E162D and E162A, a series of catalytic studies using mainly pulse radiolysis and structural studies using X-ray crystallography were performed.

Structures. In wild-type MnSOD, the side chain of Glu162 forms a hydrogen bond with the side chain of His163 from the adjacent subunit (Figure 1) (*3, 8*). This interaction is weakened in E162D MnSOD as the carboxyl group is more distant from His163 but is somewhat rescued by the intervention of a solvent molecule bridging Asp162 and His163 (Figure 5, middle). However, this interaction is completely abolished in E162A MnSOD (Figure 5, bottom). Overall, these replacements caused almost no observed changes in backbone and side chain interactions. Of note is the observation of bound sulfate molecules in the vicinity of mutated residues Asp162 and Ala162 in both mutant structures (Figure 5). Such sulfate binding sites have not been previously reported for wild-type MnSOD structures when similar 3 M ammonium sulfate precipitant solutions were used for the crystallization conditions. The sulfate ions were most likely introduced into the respective mutant MnSOD solvent channels during crystallization. The solvent molecule at position S_2 in wild-type MnSOD (Figure 1) is replaced with sulfate in the E162D MnSOD structure (Figure 5, middle). Alignment of the sulfate binding region of E162D and wild-type MnSOD indicates an opening in the structure. The sulfate binding site could correspond to a pathway for the entry of superoxide into the region of the active site cavity. The sulfate bound in E162A MnSOD is hydrogen bonded to the side chains of His30 and Tyr34, which are partially exposed to solvent (Figure 5, bottom). These bound sulfate molecules suggest enhanced mobility and/or expansion of solvent-accessible channels at the dimeric interfaces of both E162A and E162D compared to wild-type MnSOD. It should be noted sulfate was not present in the measurements of catalysis or of spectral properties of these mutants of MnSOD.

Differential scanning calorimetry showed that the main unfolding transition of E162D MnSOD (88 °C) is not significantly altered compared with that of wild-type human MnSOD (90–94 °C), consistent with the retention in the mutant of the hydrogen bond between Asp162 and His163 through an intervening solvent molecule. In contrast, this transition for E162A MnSOD is decreased to 81 °C, attributed in significant part to the removal of a stabilizing interaction with His163 from the adjacent subunit. The reduced stability, however, did not affect tetramerization of E162A MnSOD.

Visible Spectroscopy. The visible spectrum of Mn^{3+}SOD is characterized by a broad absorption in the visible region with a maximum at 480 nm (*27, 29, 30*). The pH profile of this maximum titrates with reported pK_a values of 9.3 (*30*) and 9.7 (*31*) for *E. coli* MnSOD and 9.4 (*29*) and 9.2 (this study) for human MnSOD. Although there has been some disagreement about the source of this ionization, a thorough study in *E. coli* Mn^{3+}SOD assigns this to Tyr34 (*30*) with corroborating evidence from Y34F that human Mn^{3+}SOD exhibits a pK_a near 11 significantly different from the visible spectrum of wild-type MnSOD (*29, 32*). Ionization of Tyr34 is also most likely the source of the pK_a of ~9.5 in catalysis by human MnSOD (*29, 30, 32*), although this is not without alternatives (*31*).

The mutations E162D and E162A affect this critical pK_a in the visible spectrum of human MnSOD; however, this effect appears to shift the pK_a in opposite directions for each mutant (Figure 2). The change in this pK_a could be explained in part by the effects of these mutations on the ionization of Tyr34, the side chain of which is located 6.2 Å from the carboxylate of Glu162 emanating from the adjacent subunit in wild-type MnSOD (Figure 1) (*3*). There is a hydrogen-bonded chain extending from the side chain of Glu162 to Tyr34 through His163 and solvent molecule S_2 allowing indirect interaction between Glu162 and Tyr34 (Figure 1). The side chain of Asp162 in the E162D mutant maintains an interaction with Tyr34 through a solvent-bridged interaction with His163, and the pK_a of E162D is only slightly decreased with respect to that of wild-type MnSOD (see the legend of Figure 2). In E162A MnSOD, the interaction with Tyr34 is weakened or abolished and instead solvent molecules may intervene between these two residues, although they are not specifically observed as ordered water in the crystal structure. With Glu162 replaced with Ala, there are likely smaller contributions to the changes in the pK_a of Tyr34 which in E162A has a pK_a more similar to its solution pK_a (Figure 2).

Catalysis. Replacement of the second-shell ligand Glu162 with Ala or Asp resulted in a diminished level of catalysis compared to that of human wild-type MnSOD as measured by k_1 and k_2 [eqs 1 and 2, respectively (Table 1)]. Though not essential for catalysis, Glu162 when replaced with Asp resulted in an 4−8-fold decrease in rate constants k_1 and k_2 and an 20-fold decrease when replaced by Ala. This is related to the weakened interaction between Glu162 and His163 and the possible concomitant effects on the properties of the metal and active site residues such as Tyr34. There is a precedent for substantial changes in catalysis with mutations at a second-shell ligand and at the dimeric interface. The replacement of the second-shell ligand Gln143 with Asn resulted in a 100-fold reduction in the level of catalysis and evidence of an increase in the redox potential of the active site (*33, 34*). The Y166F mutation at the dimeric interface, though not a second-shell ligand, resulted in a 10-fold decrease in catalysis [Table 1 (*10*)].

One interesting aspect of the catalytic step described by k_1 for E162D MnSOD (Figure 4) is that it appears to have a pH dependence with a value of the kinetic pK_a near 8.7 that roughly matched the pK_a of the molar absorptivity (Figure 2). E162D MnSOD with a pH dependence that appears well within the range of practicable kinetic measurements should be useful for further studies. We observed no pH dependence for the kinetic constant k_1 for E162A MnSOD in our pH range of 7.5–10.0, roughly consistent with its higher pK_a observed in the pH dependence of its visible spectrum.

There are some interesting differences noted in properties of human E162A MnSOD in this study compared with an equivalent mutant from *E. coli* MnSOD. The human mutant E162A MnSOD retains specificity for manganese and is catalytically active, although at 5–25% of the level of the human wild type (Table 1). Additionally, it remains a tetramer in solution. This is in contrast to the equivalent mutation in *E. coli*, E170A MnSOD, which results in complete loss of catalytic activity and dimer destabilization in solution and is accompanied by a change in specificity to $Fe^{2+/3+}$ (*12*). Comparison of the crystal structures of the human and *E. coli* forms of MnSOD shows nearly superimposable residues for the ligands of the metal and side chains of Tyr34 and His30. However, there is a substructure of the active site that is considerably different for these two forms of MnSOD, and this offers significant clues about the different responses of the human and *E. coli* forms of MnSOD to replacements at residue 162. Included in the set of interactions that forms the dimeric interface of human MnSOD is a stabilizing, van der Waals interaction between Phe66 and Gln119 (3.5 Å) that is present, though in a different orientation in the *E. coli* enzyme. This specific difference, rather far from the manganese, is one of many interactions at the dimer interface that is likely to account for differences in properties of MnSOD from humans and *E. coli* (*35*).

Product Inhibition. Product inhibition is a prominent feature of catalysis by human MnSOD (*28, 29*). The maximal values of k_0/[E], zero-order rate constant for product inhibition at steady state, for E162D and E162A (270 and 190 s^{-1}, respectively) were diminished compared to that of wild-type MnSOD (500 s^{-1}). This measures the enhanced product inhibition of the two mutants compared with the wild type at steady state. Moreover, there were significant decreases in k_3 and k_4 (eqs 3 and 4) describing this inhibition by E162D and E162A compared with-type MnSOD (Table 1). The greater level of product inhibition for E162D and E162A is reflected in the values of the k_2/k_3 ratio in the two mutants. This is a gating ratio that determines the extent of reaction that proceeds to catalysis versus inhibition (eq 2 vs eq 3). The values of the gating ratios for E162D and E162A (~0.6) are consistent with enhanced flux in the mechanism through the pathway to inhibition (k_3 of eq 3) and the greater product inhibition k_0/[E] observed for the mutants. In addition, the side chain of Glu162 appears to mediate dissociation of the product-inhibited complex as evidenced by the smaller values for k_4 for both E162A and E162D compared with the wild type (Table 1). Moreover, the E162A mutant is unusual in exhibiting a pH-dependent value for k_4. This provides another avenue for future investigation since neither the structure of the inhibited complex nor its mechanism of dissociation is known.

In summary, these data emphasize the role of the dimeric interface in human MnSOD. The side chain of Glu162 that extends across this interface to interact with the active site of an adjacent residue influences many properties of MnSOD, including structure, stability, catalysis, and inhibition. As mutant forms of MnSOD are prepared as possible

antiproliferative agents, such as H30N MnSOD which exhibits less product inhibition than the wild type (*36*), we should expect that alteration of Glu162 and possibly other residues at the dimeric interface is likely to slow catalysis and enhance product inhibition. In seeking explanations for differences in properties between MnSOD forms from bacteria and animals, the dimeric interface is a likely source.

ACKNOWLEDGMENT

We thank Dr. Omjoy Ganesh for helpful discussions regarding calorimetric data analysis.

SUPPORTING INFORMATION AVAILABLE

Differential scanning calorimetry profiles of apparent excess specific heat versus temperature for the enzymes studied herein. This material is available free of charge via the Internet at http://pubs.acs.org.

REFERENCES

1. Fridovich, I. (1997) Superoxide anion radical ($O_2^{-\bullet}$), superoxide dismutases, and related matters. *J. Biol. Chem. 272*, 18515–18517.
2. Miller, A. F. (2004) Superoxide dismutase: Active sites that save, but a protein that kills. *Curr. Opin. Chem. Biol. 8*, 162–168.
3. Borgstahl, G. E., Parge, H. E., Hickey, M. J., Beyer, W. F., Jr., Hallewell, R. A., and Tainer, J. A. (1992) The structure of human mitochondrial manganese superoxide dismutase reveals a novel tetrameric interface of two 4-helix bundles. *Cell 71*, 107–118.
4. Edwards, R. A., Baker, H. M., Whittaker, M. M., Whittaker, J. W., Jameson, G. B., and Baker, E. N. (1998) Crystal structure of *Escherichia coli* manganese superoxide dismutase at 2.1 Angstrom resolution. *J. Biol. Inorg. Chem. 3*, 161–171.
5. Mizuno, K., Whittaker, M. M., Bachinger, H. P., and Whittaker, J. W. (2004) Calorimetric studies on the tight binding metal interactions of *Escherichia coli* manganese superoxide dismutase. *J. Biol. Chem. 279*, 27339–27344.
6. Greenleaf, W. B., Perry, J. J., Hearn, A. S., Cabelli, D. E., Lepock, J. R., Stroupe, M. E., Tainer, J. A., Nick, H. S., and Silverman, D. N. (2004) Role of hydrogen bonding in the active site of human manganese superoxide dismutase. *Biochemistry 43*, 7038–7045.
7. Wagner, U. G., Pattridge, K. A., Ludwig, M. L., Stallings, W. C., Werber, M. M., Oefner, C., Frolow, F., and Sussman, J. L. (1993) Comparison of the crystal structures of genetically engineered human manganese superoxide dismutase and manganese superoxide dismutase from *Thermus thermophilus*: Differences in dimer-dimer interaction. *Protein Sci. 2*, 814–825.
8. Whittaker, M. M., and Whittaker, J. W. (2000) Recombinant superoxide dismutase from a hyperthermophilic archaeon, *Pyrobaculum aerophilium*. *J. Biol. Inorg. Chem. 5*, 402–408.
9. Borgstahl, G. E., Parge, H. E., Hickey, M. J., Johnson, M. J., Boissinot, M., Hallewell, R. A., Lepock, J. R., Cabelli, D. E., and Tainer, J. A. (1996) Human mitochondrial manganese superoxide dismutase polymorphic variant Ile58Thr reduces activity by destabilizing the tetrameric interface. *Biochemistry 35*, 4287–4297.
10. Hearn, A. S., Fan, L., Lepock, J. R., Luba, J. P., Greenleaf, W. B., Cabelli, D. E., Tainer, J. A., Nick, H. S., and Silverman, D. N. (2004) Amino acid substitution at the dimeric interface of human manganese superoxide dismutase. *J. Biol. Chem. 279*, 5861–5866.
11. Quint, P., Ayala, I., Busby, S. A., Chalmers, M. J., Griffin, P. R., Rocca, J., Nick, H. S., and Silverman, D. N. (2006) Structural mobility in human manganese superoxide dismutase. *Biochemistry 45*, 8209–8215.
12. Whittaker, M. M., and Whittaker, J. W. (1998) A glutamate bridge is essential for dimer stability and metal selectivity in manganese superoxide dismutase. *J. Biol. Chem. 273*, 22188–22193.
13. Borgstahl, G. E. O., Pokross, M., Chehab, R., Sekher, A., and Snell, E. H. (2000) Cryo-trapping the six-coordinate, distorted-octahedral active site of manganese superoxide dismutase. *J. Mol. Biol. 296*, 951–959.
14. Abreu, I. A., Hearn, A., An, H., Nick, H. S., Silverman, D. N., and Cabelli, D. E. (2008) The Kinetic Mechanism of Manganese-Containing Superoxide Dismutase from *Deinococcus radiodurans*: A Specialized Enzyme for the Elimination of High Superoxide Concentrations. *Biochemistry 47*, 2350–2356.
15. Carlioz, A., and Touati, D. (1986) Isolation of superoxide dismutase mutants in *Escherichia coli*: Is superoxide dismutase necessary for aerobic life? *EMBO J. 5*, 623–630.
16. Leveque, V. J., Vance, C. K., Nick, H. S., and Silverman, D. N. (2001) Redox properties of human manganese superoxide dismutase and active-site mutants. *Biochemistry 40*, 10586–10591.
17. Schwartz, H. (1981) Free radicals generated by radiolysis of aqueous solutions. *J. Chem. Educ. 58*, 101–105.
18. Rabani, J., and Nielsen, S. O. (1969) Absorption spectrum and decay kinetics of superoxide in aqueous solutions by pulse radiolysis. *J. Phys. Chem. 73*, 3736–3744.
19. Cabelli, D. E., Guan, Y., Leveque, V., Hearn, A. S., Tainer, J. A., Nick, H. S., and Silverman, D. N. (1999) Role of tryptophan 161 in catalysis by human manganese superoxide dismutase. *Biochemistry 38*, 11686–11692.
20. Otwinowski, Z., and Minor, W. (1997) Processing of X-ray Diffraction Data Collected in Oscillation Mode. *Methods Enzymol. 276*, 307–326.
21. Quint, P., Reutzel, R., Mikulski, R., McKenna, R., and Silverman, D. N. (2006) Crystal structure of nitrated human manganese superoxide dismutase: Mechanism of inactivation. *Free Radical Biol. Med. 40*, 453–458.
22. Brunger, A. T., Adams, P. D., Clore, G. M., DeLano, W. L., Gros, P., Grosse-Kunstleve, R. W., Jiang, J. S., Kuszewski, J., Nilges, M., Pannu, N. S., Read, R. J., Rice, L. M., Simonson, T., and Warren, G. L. (1998) Crystallography & NMR system: A new software suite for macromolecular structure determination. *Acta Crystallogr. D54*, 905–921.
23. Emsley, P., and Cowtan, K. (2004) Coot: Model-building tools for molecular graphics. *Acta Crystallogr. D60*, 2126–2132.
24. Fridovich, I. (1997) Superoxide anion radical, superoxide dismutases, and related matters. *J. Biol. Chem. 272*, 18515–18517.
25. McAdam, M. E., Fox, R. A., Lavelle, F., and Fielden, E. M. (1977) A pulse-radiolysis study of the manganese-containing superoxide dismutase from *Bacillus stearothermophilus*. A kinetic model for the enzyme action. *Biochem. J. 165*, 71–79.
26. Miller, A.-F., Padmakumar, D., Sorkin, D. L., Karapetian, A., and Vance, C. (2003) Proton-coupled electron transfer in FeSOD and MnSOD. *J. Inorg. Biochem. 93*, 71–83.
27. Bull, C., Niederhoffer, E. C., Yoshida, T., and Fee, J. A. (1991) Kinetic Studies of Superoxide Dismutases: Properties of the Manganese-Containing Protein from *Thermus thermophilus*. *J. Am. Chem. Soc. 113*, 4069–4076.
28. Hearn, A. S., Stroupe, M. E., Cabelli, D. E., Lepock, J. R., Tainer, J. A., Nick, H. S., and Silverman, D. N. (2001) Kinetic analysis of product inhibition in human manganese superoxide dismutase. *Biochemistry 40*, 12051–12058.
29. Hsu, J. L., Hsieh, Y., Tu, C., O'Connor, D., Nick, H. S., and Silverman, D. N. (1996) Catalytic properties of human manganese superoxide dismutase. *J. Biol. Chem. 271*, 17687–17691.
30. Maliekal, J., Karapetian, A., Vance, C., Yikilmaz, E., Wu, Q., Jackson, T., Brunold, T. C., Spiro, T. G., and Miller, A. F. (2002) Comparison and contrasts between the active site pKs of Mn-superoxide dismutase and those of Fe-superoxide dismutase. *J. Am. Chem. Soc. 124*, 15064–15075.
31. Whittaker, M. M., and Whittaker, J. W. (1997) Mutagenesis of a proton linkage pathway in *Escherichia coli* manganese superoxide dismutase. *Biochemistry 36*, 8923–8931.
32. Guan, Y., Hickey, M. J., Borgstahl, G. E., Hallewell, R. A., Lepock, J. R., O'Connor, D., Hsieh, Y., Nick, H. S., Silverman, D. N., and Tainer, J. A. (1998) Crystal structure of Y34F mutant human mitochondrial manganese superoxide dismutase and the functional role of tyrosine 34. *Biochemistry 37*, 4722–4730.
33. Leveque, V. J., Stroupe, M. E., Lepock, J. R., Cabelli, D. E., Tainer, J. A., Nick, H. S., and Silverman, D. N. (2000) Multiple replacements of glutamine 143 in human manganese superoxide dismutase: Effects on structure, stability, and catalysis. *Biochemistry 39*, 7131–7137.
34. Hsieh, Y., Guan, Y., Tu, C., Bratt, P. J., Angerhofer, A., Lepock, J. R., Hickey, M. J., Tainer, J. A., Nick, H. S., and Silverman,

D. N. (1998) Probing the active site of human manganese superoxide dismutase: The role of glutamine 143. *Biochemistry 37*, 4731–4739.

35. Zheng, J., Domsic, J. F., Cabelli, D., McKenna, R., and Silverman, D. N. (2007) Structural and kinetic study of differences between human and *Escherichia coli* manganese superoxide dismutases. *Biochemistry 46*, 14830–14837.
36. Davis, C. A., Hearn, A. S., Fletcher, B., Bickford, J., Garcia, J. E., Leveque, V., Melendez, J. A., Silverman, D. N., Zucali, J., Agarwal, A., and Nick, H. S. (2004) Potent anti-tumor effects of an active site mutant of human manganese-superoxide dismutase. Evolutionary conservation of product inhibition. *J. Biol. Chem. 279*, 12769–12776.
37. Hearn, A. S., Stroupe, M. E., Cabelli, D. E., Ramilo, C. A., Luba, J. P., Tainer, J. A., Nick, H. S., and Silverman, D. N. (2003) Catalytic and structural effects of amino acid substitution at histidine 30 in human manganese superoxide dismutase: Insertion of valine Cγ into the substrate access channel. *Biochemistry 42*, 2781–2789.

BI7024518